IRIS Team's Mechanical and Electrical Description

Dwi Ananda Akbar Pabelan[1], Abiyyu Ravely Wijaya[1], Alvaro[1], Andika Rizky Noval Nugraha[1], Ari Rangga Prasetio[1], Fauzi Gaga Ardilla[1], Galuh Rifa'i Najmudin[1], Givaro Gama[1], Muhammad Fahridho Nurrahman[1], Muhammad Syauqi Rofii[1], Izza Azizah[1], and Zidan Maulana Ahsan[1]

Workshop Laboratory, ITS Robotics Centre, Institut Teknologi Sepuluh Nopember, Surabaya 60111, Indonesia iris.krsbi@gmail.com
Home page: iris.its.ac.id
{iris.krsbi@gmail.com}

1 Main Structure

The main structure of this robot consists of three DC Servo and triple Omni wheel motors as the main drive, a pair of passive rotary encoders, a pair of free wheels, and a capacitor for the solenoid.

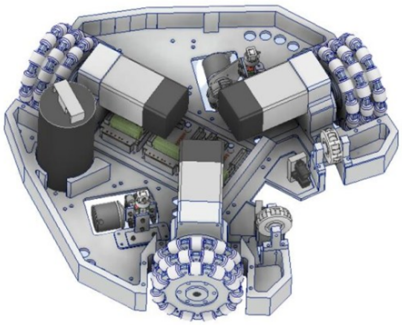

Fig. 1: Main Structure

1.1 Maximum Linear Velocity

The robot's propulsion system employs a three-wheel holonomic drive configuration powered by Leadshine ACM602V36 AC Servo motors (3000 RPM). Power is transmitted through a 1:4 gear ratio to 12.5 cm diameter omni-wheels. The maximum linear speed ($v_{\max}$) is determined by the following formula:

$$v_{\max} = \frac{\pi \cdot D(n_{\text{motor}}/G)}{60}$$

With $D = 0.125$, $n_{\text{motor}} = 3000$ RPM, and $G = 4$, the theoretical maximum speed is **4.9 m/s**. To ensure control stability for the robot's **39.6 kg** mass, the current operational wheel speed is set to **450 RPM**, resulting in an operational linear speed of:

$$v_{\text{ops}} = \frac{\pi \cdot 0.125 \cdot 450}{60} \approx 2.95\,\text{m}\,\text{s}^{-1}$$

1.2 Wheel Torque and Driving Force

The available wheel torque is a critical parameter that determines the robot's ability to accelerate, resist external disturbances, and maintain stable motion under load. The torque produced by each wheel is amplified by the gearbox reduction ratio, allowing the motor to generate sufficient traction force despite the robot's relatively large mass of 39.6 kg. The output wheel torque (τ_{wheel}) is calculated using the following relationship:

$$\tau_{\text{wheel}} = \tau_{\text{motor}} \cdot G \cdot \eta$$

Using the nominal torque of the Leadshine ACM602V36 motor of 0.64 N m, a gear ratio of 4, and an assumed gearbox efficiency of 90%, the resulting wheel torque is:

$$\tau_{\text{wheel}} = 0.64 \cdot 4 \cdot 0.9 = 2.30\,\text{N}\,\text{m}$$

This torque is then converted into linear driving force at the wheel-ground interface. Since torque is defined as force multiplied by radius, where $r = 0.0625$ m is the wheel radius. The traction force generated by each wheel is determined as:

$$F_{\text{wheel}} = \frac{2.30}{0.0625} = 36.8\,\text{N}$$
$$F_{\text{total}} = 3 \cdot F_{\text{wheel}} = 110.4\,\text{N}$$

This total driving force allows the robot to accelerate efficiently while maintaining precise control during dynamic maneuvers such as ball pursuit, sudden direction changes, and defensive positioning.

1.3 Robot Acceleration

The available driving force directly determines the robot's linear acceleration capability, which is essential for rapid response during dynamic gameplay situations such as intercepting the ball, repositioning, and defensive maneuvers. According to Newton's Second Law of Motion, acceleration is proportional to the applied force and inversely proportional to the robot mass. To further evaluate the robot's responsiveness, the time required to reach the operational maximum velocity of 2.95 m/s can be estimated using:

$$t = \frac{v}{a}$$

The calculated result indicates that the robot reaches its operational velocity of **2.95 m/s in approximately 1.06 seconds**, confirming that the drive system provides sufficient force to achieve rapid acceleration while maintaining traction and motion stability.

1.4 Traction Analysis

In addition to motor torque capability, it is essential to verify that the generated driving force does not exceed the maximum traction force between the omni-wheels and the field surface. If the applied force exceeds the traction limit, wheel slip may occur, resulting in loss of control and reduced motion accuracy. The maximum traction force is determined using the friction model:

$$F_{\text{friction}} = \mu \cdot m \cdot g$$

The maximum available traction force between the omni-wheels and the field surface is calculated to be approximately **233 N**, which represents the upper limit of force that can be transmitted without causing wheel slip. This value is significantly higher than the total driving force generated by the motors, ensuring that the robot maintains sufficient grip and stable motion under normal operating conditions.

1.5 Configuration Drive System

This configuration provides optimal torque for instant acceleration while ensuring precise braking, allowing the robot to maneuver with high accuracy without significant wheel slippage.

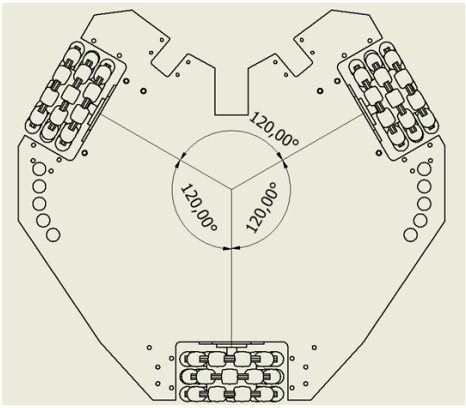

Fig. 2: Holonomic Drive System

The robot's drive system utilizes a three-wheel holonomic configuration, with each omni-wheel symmetrically arranged around the robot's center of mass. The wheels are positioned at 120 degree offset from one another to enable full holonomic mobility, allowing the robot to perform simultaneous translation in any direction and rotation. The relationship between the robot's linear velocity (vx, vy)

and angular velocity (ω) relative to each wheel's speed (Vn) is defined by the following kinematic matrix:

$$V_n = -v_x \sin \alpha_n + v_y \sin \alpha_n + \omega \cdot R$$

Where α_n represents the angular position of each wheel ($\alpha_1 = 0, \alpha_2 = 120, \alpha_3 = 240$) and R is the distance from the center of mass to the wheel center. This 120 degree configuration is chosen to ensure the 39.6 kg mass is evenly distributed across the three ACM602V36 motors. This minimizes wheel slippage during rapid acceleration and ensures that the resultant thrust remains stable at every movement angle across the field.

1.6 Servo Motor Driver

To drive the motor, Elmo Motion Control's Sol-Gui/25/100 Simpliq Servo Driver. The driver can delivers up to 4.8 kW of continuous power or 5.4 kW of peak power.

Fig. 3: Solo Guitar Servo Driver

CAN busses are used to ensure stable communication with the main PC with CANopen protocol.

2 Robot Frame

The Robot Frame is the structure of the robot that supports the secondary structure upwards and the placement of electronic components. This robot structure is designed with several profiles to reduce the weight of the robot and increase the flexibility of electronic component placement in case of component design changes and cable management.

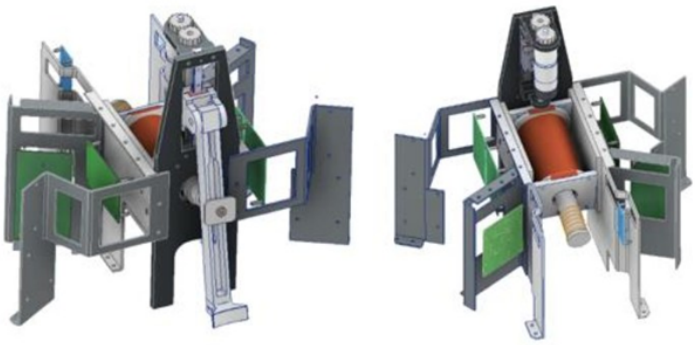

(a) Front View (b) Back View

Fig. 4: Robot Structure

3 Ball Handler

Ball Handlers on the striker robot are attached to the main structure. The ball handler's system is integrated with angle sensors and hydraulic dampers to maintain stability in dribbling.

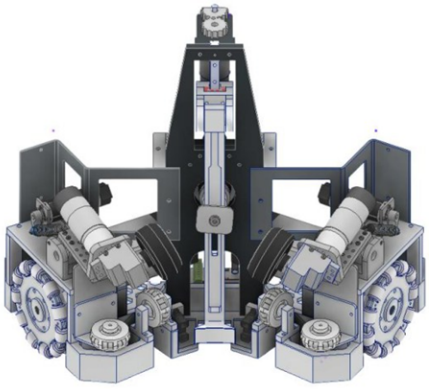

Fig. 5: Ball Handler Mechanism

3.1 Ball Handler's Mechanism

The ball handling mechanism is designed with a tilt angle of 23° to 24° to optimize ball control during high-speed maneuvers. Physically, this angle determines the distribution of force exerted by the dribbler motors onto the ball's surface. Using

a trigonometric approach, the normal force (F_n) pressing the ball to the floor is formulated as $F_n = F_{\text{total}} \cdot \cos\theta$, while the horizontal force ($F_h = F_{\text{total}} \cdot \sin\theta$). By selecting an angle θ between 23-24 degrees, the $cos\theta$ value remains dominant (≈ 0.91), ensuring that most of the motor power is converted into downward pressure. This pressure effectively "locks" the ball, preventing it from bouncing when receiving hard passes or when the 39.6 kg robot performs sudden deceleration. The use of silicon rubber wheels further enhances this efficiency through a high friction coefficient, which instantaneously transfers motor torque into backspin to maintain stable ball possession. The ball handler is powered by a DC PG36 planetary gearbox motor, chosen for its high torque characteristics and reliability under load. Power is transmitted to silicon wheels via a 90-degree bevel gear system. This mechanical layout allows vertical or longitudinal motor orientation, optimizing the internal space for the solenoid kicking system and maintaining a balanced distribution of the robot's 39.6 kg mass. The system operates at a wheel speed of 120 RPM, generating a steady angular velocity of approximately 12.57 rad/s. The combination of the planetary gearbox's torque and the bevel gear transmission ensure consistent friction against the ball, providing the necessary backspin to secure the ball during aggressive maneuvers or sudden changes in direction.

3.2 Ball Handler's Electronic

The ball handler motor are driven using custom H-Bridge Drivers that can support 40 V and 20 A with an external MOSFET. The driver also includes extra feature like current sensor, MCU ground isolation, and CAN Bus support with CANopen protocol.

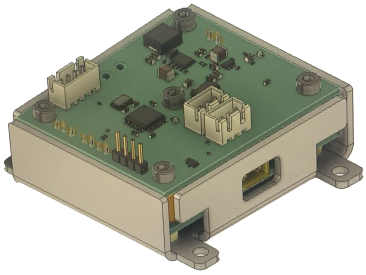

Fig. 6: Brushed DC Motor Driver

Aside from the PG36's 7ppr incremental encoder for speed control, there are other sensors to detect the presence of a ball. First, there are two IR sensors to detect the distance of the ball. In addition, there are two potentiometers to detect the handler's angle. Both sensors control the handler behavior and help the ball flow naturally.

4 Kicking Mechanism

The kicking mechanism uses a solenoid that is integrated with a lifting mechanism to adjust the height of the ball kick and a return spring to return the plunger to its initial position.

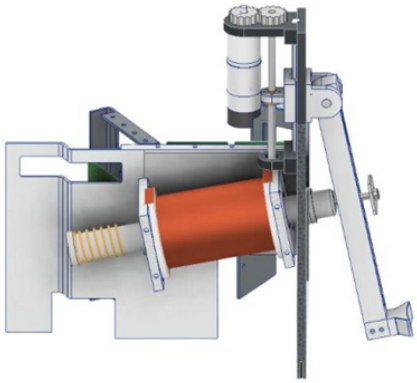

Fig. 7: Kicking Mechanism

The robot's kicking mechanism employs a custom electromagnetic solenoid powered by a 4700uF capacitor bank with an operating voltage of 350V to 450VDC. Generating up to 376 Joules of potential energy, the system achieves a maximum ball speed of 10m/s. The solenoid coil consists of 1,120 turns of 1mm diameter copper wire (80 turns x 14 layers) to optimize magnetic flux while minimizing thermal resistance. Integrated with a lifting mechanism, the system precisely adjusts the impact point: a center contact for torque-free flat kicks, and a lower contact for loft kicks that utilize backspin torque for trajectory stability. The robot's 39.6 kg mass provides sufficient inertia to dampen recoil forces, ensuring shot accuracy and maintaining localization stability during high-power discharge.

The shooting mechanism utilizes a custom-designed solenoid consisting of 1,120 turns (14 layers) powered by a 400V capacitor discharge system. To evaluate its performance, a work-energy analysis was conducted, where the system delivers a total work (W) of 37.5 Joules. Based on the work-distance relation, $W = F_{\text{avg}} \cdot d$, the solenoid generates an average driving force (F_{avg}) of 750 N (168.6 lbf) over a 0.05 m plunger stroke, with a magnetic peak force (F_{solenoid}) reaching 1,000 N (224.8 lbf). This energy is transferred through a 250 mm lever arm mounted at a 60 angle to facilitate chip kicks. Upon collision with a standard 0.45 kg ball, the mechanism exerts a peak impact force ($F_{\text{peakimpact}}$) of approximately 1,250 N (281.0 lbf), calculated through the impulse-momentum theorem.

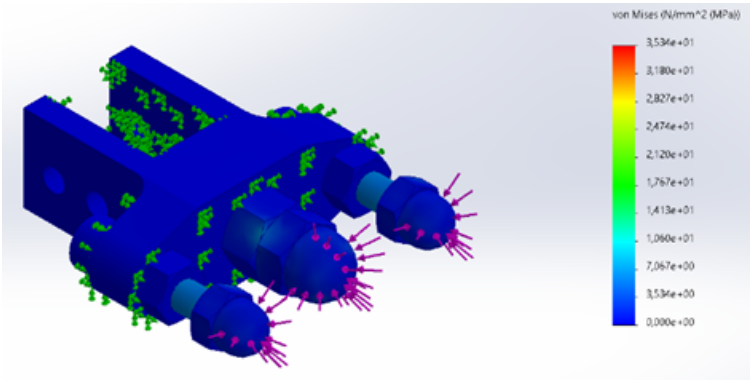

(a) Stress

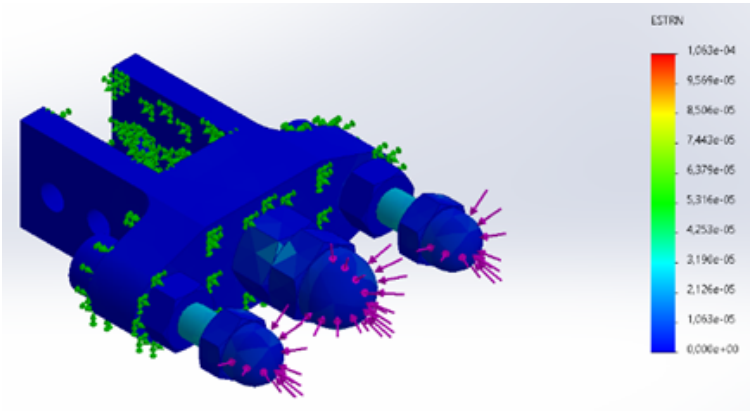

(b) Strain

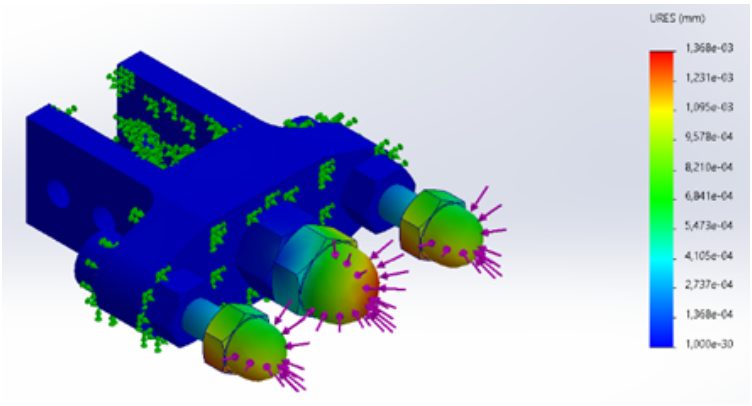

(c) Displacement

Fig. 8: Kicker Von Mises Diagram

Under an applied load of 1250 N, the static simulation in Figure 8 shows that the maximum von Mises stress is concentrated at the cap nut directly subjected to the impact, while the main shoe structure experiences much lower stress, indicating effective load transfer. The largest displacement and strain are also localized at the cap nut, with a maximum displacement on the order of 10^3 mm and negligible deformation in the fixed regions, confirming that the structure behaves rigidly. When compared with the yield strength of stainless steel (approximately 200–250 MPa), the maximum stress of about 35 MPa is significantly lower, resulting in a safety factor greater than 6. These results indicate that deformation is highly localized and that the cap nut and fastening components remain within the elastic range and are structurally safe under the applied load.

The capacitor voltages are provided by a flyback transformer from the 40 V source to a 450 V output. The transformer is used in the boost converter to provide galvanic isolation between the 40 V battery supply from the side of the 450 V high-voltage capacitor. Compared to the previous model, this new solenoid driver board is more efficient and features a smaller and fully analog design without the need for a microcontroller.

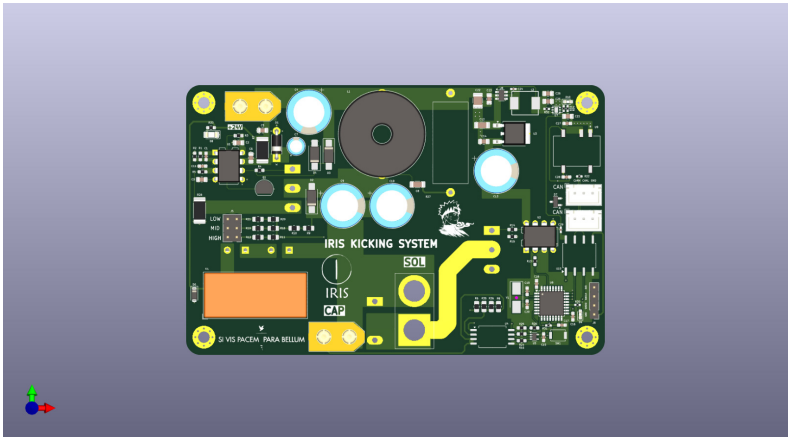

Fig. 9: Solenoid Control and Voltage Booster

Additionally, the new board includes a dummy load that safely discharges the capacitor when the booster system is deactivated.

5 Secondary Structure

The Secondary Structure is designed to have a profile that provides flexibility for cable management of electronic components on our robot. This secondary structure is a platform to place batteries, some electronic components, and the lifting kicker mechanism on our robot.

(a) Front View (b) Back View

Fig. 10: Secondary Structure

6 Main PC

Intel® NUC Kit NUC6i7KYK 6th generation is used as the main brain of the robot. The robot has Intel Core i7-6770HQ processor (2.6 GHz up to 3.5 GHz Turbo, Quad-Core 6MB cache, 45W TDP) with Iris Pro graphic 580.

Fig. 11: Main PC

For the operating system, we use Linux Ubuntu 20.04 to support ROS Noetic. Which is the robot operating system that we used.

7 Robot Visions

Our striker robot detects the environment using 2 cameras that have their functions. The omnidirectional camera is the main camera, and the front camera is the support camera.

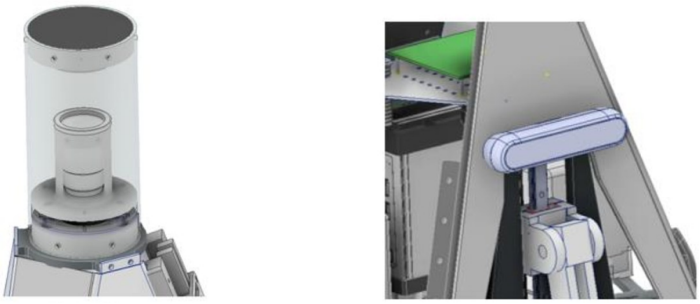

(a) Omnidirectional Camera (b) Front Camera

Fig. 12: Robot Visions

The omnidirectional camera uses Logitech C920 Webcam with 3 Megapixel camera that can record 1080p video in 30 fps and has 78° diagonal field of view (dFoV). The 360° vision is achieved with convex mirror on top of the camera.

8 Hardware Flow

In general, the main control of the robot is the PC. The motors are controlled by CAN Bus from PC via Ethernet-to-CAN device.

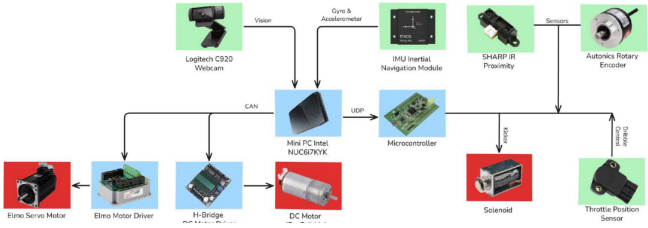

Fig. 13: Hardware Flowchart

Important sensor such as camera and the Inertial Measuring Unit (IMU) is fed directly to PC via USB Port. Other sensors will be read with MCU (which is STM32) and sent to PC via Ethernet UDP.

9 Power Distribution

Two 5S2P (5 cells in series, 2 cells in parallel) 18650 Li-Ion battery (18.5 V nominal voltage) LXT cordless battery packs are used to power the robot. With the two batteries in series, the supply voltage ranged from 37 V to 40 V which is sufficient to power the 36V main drive servo motor.

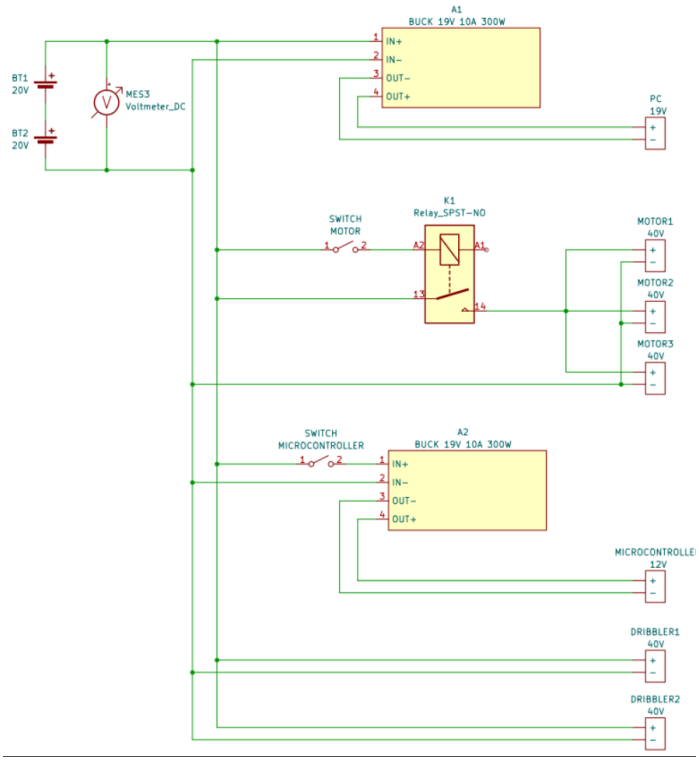

Fig. 14: Power Distribution Schematic

The PC is powered with 40 V to 19 V Buck Converter and the MCU is powered with 40 V to 12 V and then 12 V to 5 V Buck Converter. The 5 V and 12 V supply are also used to power other sensors.

10 Robot Materials and Specification

The following table outlines the material specifications for the robot's structural and functional components. The selection of materials is based on a balance between high structural integrity, weight efficiency, and precise mechanical performance to ensure optimal durability during high-speed maneuvers and gameplay.

No	Part	Specification
1	Base	Aluminium CNC
2	Omni wheel	Aluminium sheet
3	Dribble arms	Aluminium
4	Kicker	Aluminium CNC
5	Battery bracket	ABS/PETG/PLA filament
6	Cover	Aluminium sheet
7	Support	Carbon
8	Roda dribble	Rubber
9	Camera bracket	Nylon
10	Cover Camera	Polypropylene
11	Plunger	Steel
12	Peer	Steel
13	Linear rail	Steel and aluminium

Table 1: Materials Used in Striker

No	Dimension	Value
1	Length	51.3cm
2	Width	50.7cm
3	Height	77.2cm
4	Mass	39.6cm
5	Base 2 Height	25.2cm
6	Base 3 Height	44.3cm

Table 2: Robot Dimensions

References

1. Lin-Bo Luo, In-Sung Koh, Kyeong-Yuk Min, Jun Wang, Jong-Wha Chong: Low-cost implementation of bird's-eye view system for camera-on-vehicle. 2010 Digest of Technical Papers International Conference on Consumer Electronics (ICCE). (2010).
2. Duda, R.O., Hart, P.E.: Use of the hough transformation to detect lines and curves in pictures. Communications of the ACM. 15, 11–15 (1972).
3. Ding, Y., Xu, Z., Zhang, Y. et al. Fast lane detection based on bird's eye view and improved random sample consensus algorithm. Multimed Tools Appl 76, 22979–22998 (2017).